molecular pharmaceutics

pubs.acs.org/molecularpharmaceutics

Article

A Universal Tag To Supercharge Proteins for Cytosolic Delivery

Yanan Quan, Weina Jing, Lei Peng, Wanrong Yang, and Wanyi Tai*

Cite This: *Mol. Pharmaceutics* 2026, 23, 3722−3731

Read Online

ACCESS | Metrics & More | Article Recommendations | Supporting Information

ABSTRACT: Supercharged proteins are some naturally occurring proteins that bear an abnormally high number of charged amino acids but can fold correctly and function normally. Owing to the nanoscale three-dimensional charge distribution associated with folding, the superpositively charged proteins possess the ability to rapidly enter mammalian cells with a potency much greater than cell-penetrating peptides and protein transduction domains. To harness the advantage, some proteins have been extensively mutated at their surface-exposed residues to generate "supercharged" variants such as +36GFP. Despite its effectiveness, this approach is time-consuming and only applicable to a few proteins that can tolerate the massive mutagenesis. Here, we proposed a tagging strategy to supercharge proteins and expand its application for the cytosolic delivery of proteins. Using the pan-protein binding ability of Coomassie brilliant blue (CBB), we developed a CBB-bearing cationic peptide CBB-R8 that can anchor on the protein surface and supercharge proteins without mutagenesis. The charge density of tagged proteins can be finely tuned by varying the tag/protein molar ratio, thus achieving a superior delivery efficiency to the cytosol than the canonical +36GFP. Mechanism studies revealed that the tagged protein could instantly and directly access the cytosol with little participation of endocytic pathways, resulting in the majority of delivered proteins being located in the cytosol. Moreover, the tagged proteins were discharged in the cytosol and return to biological functions after delivery, capable of catalyzing, blocking, and manipulating diverse targets inside cells. In conclusion, this simple plug-and-charge methodology greatly facilitates the preparation of supercharged proteins and expands its application to more intracellular targets.

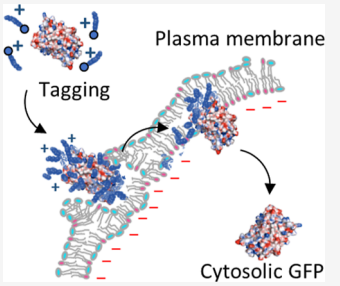

KEYWORDS: *supercharged protein, cytosolic delivery, intracellular targets, tagging, CBB*

INTRODUCTION

Supercharged proteins are a class of naturally occurring or engineered proteins that have an abnormally high number of net charges on the surface.[1] They can be either positive or negative, depending on the counterbalance between cationic and anionic amino acids in sequences. Owing to the unusual physiochemistry, supercharged proteins possess some attractive properties that have a broad application in the fields of material science, protein biology, drug delivery, and gene therapy.[1−3] It was reported that supercharged proteins have excellent water solubility and antiaggregation ability, which can be used for interfacial coatings, assembly of bioliquids, amyloid resolving,[4] protein refolding,[5,6] high-concentration storage,[7] and even antiviral therapy.[8−10] By supercharging, some characteristics of proteins can be improved and new functions can be achieved.[11] One particularly interesting function is the cell-penetrating ability.[12] It was reported that the cationic and folded scaffold enables supercharged proteins to enter mammalian cells more easily than unstructured cell penetrating peptides (CPPs).[13] Since the vast majority of biological targets encoded by the human genome are intracellular, this function opens a new avenue for protein therapeutics to manipulate targets inside cells.[14,15]

In nature, proteins are generally electrically neutral. The charged side chains are distributed broadly on the protein surface but mostly form ion pairs, thus making proteins charge-neutral. This feature is important for proteins to condense chains, fold correctly, and bind antigens. Nevertheless, Cronican et al. discovered that approximately 0.8% of the human proteome (104 entries in 13,417 human proteins) bears unusually high net positive charges (>1.27 net charges/kDa molecular weight).[16] Most of these naturally occurring proteins can fold correctly in the supercharged state and penetrate cells as part of their native biological functions, such as the histone proteins that involves the cell penetration and nuclear import.[17,18] It is an important discovery because cytosolic delivery is the main obstacle that impedes the expansion of protein therapeutics to intracellular targets.[19] To harness the supercharging advantages, the Liu group engineered green fluorescent protein (GFP) to a "supercharged" state by replacing the solvent-exposed residues with basic amino acids (Lys and Arg).[20] This positively charged GFP variant, namely the well-known +36GFP, retains the correct fold and function (the green fluorescence) as its parent. Importantly, supercharged +36GFP is able to efficiently pass

Received: February 10, 2026
Revised: May 23, 2026
Accepted: May 27, 2026
Published: June 3, 2026



ACS Publications

© 2026 American Chemical Society

https://doi.org/10.1021/acs.molpharmaceut.6c00191
Mol. Pharmaceutics 2026, 23, 3722−3731

Downloaded from pubs.acs.org/mpohbp/article-pdf/23/7/3722/6537496/acs.molpharmaceut.6c00191.pdf by WUHAN UNIV user on 20 September 2026

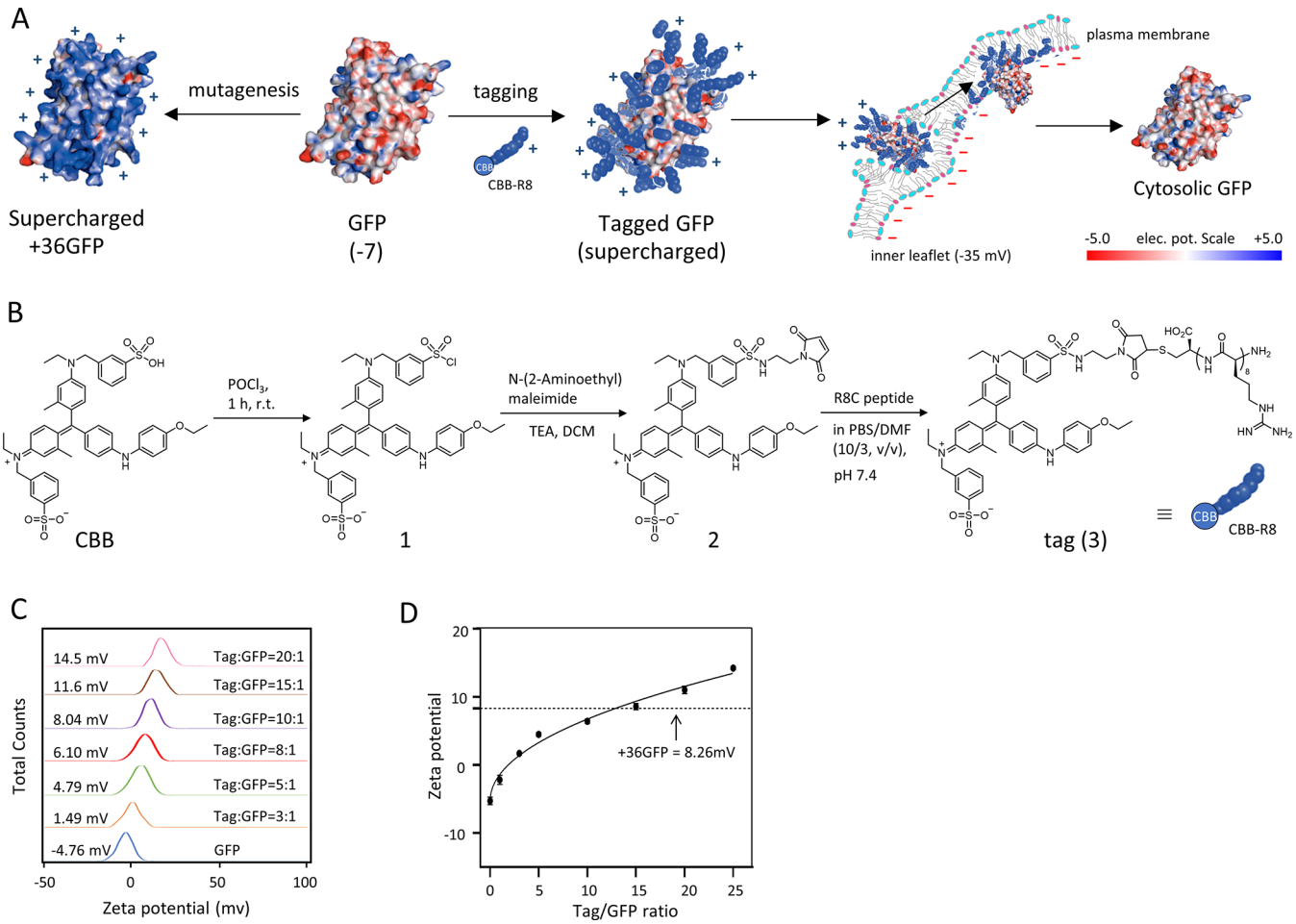

Figure 1. Cytosolic delivery of proteins by supercharging with tags. (A) Graphic illustration of the tagging approach to supercharge green fluorescent protein (GFP) through the cell membrane in comparison with the canonical +36GFP. (B) The synthetic route of tag. The bifunctional tag contains a cationic R8 peptide and a CBB moiety to anchor peptides on the protein surface. (C) Analysis of zeta potentials after titrating GFP with varying tag/protein ratios. (D) The correlation between zeta potential and ratio values. The zeta potential of tagged GFP can surpass +36GFP at a moderate ratio.

through the cell membrane by itself, and even with its cargos.[21] Besides GFP, some other proteins such as GST, Ceru, PfTrx, and nanobody could also be genetically supercharged, as reported by several laboratories independently.[22−24]

It is worth noting that reengineering protein surfaces to exhibit high net charges is a picky task. The Coulombic repulsion might destabilize the folded state of proteins when suboptimal mutations were introduced. Several in-silico methods, for examples, the Rosetta and AvNAPSA models, have been developed to guide the surface mutating strategy.[25] Nevertheless, surface mutation is not a universal approach to all proteins as the reduced thermal stability and compromised enzymatic activity have been reported in some supercharging examples.[1] By comparison, genetic fusion with cationic peptides is a more feasible strategy to supercharge proteins.[26−28] By varying the length and sequences of cationic peptides, the net positive charges ranging from +3 to +60 could be incorporated into cargo proteins without impact on biological activity.[29] However, in this case, the cationic charges always crowd in a particular region of fusion protein, making its electrostatic topography quite different from the surface-mutated comparators. A huge difference in cell penetration, leading up to ∼100-fold greater potency by the latter, has been reported.[21] In addition, both genetic fusion and surface mutation require a laborious effort to clone and express proteins, which is time-consuming and low in efficiency. Therefore, an impactful and simple method to supercharge proteins is needed to expand their application for intracellular targeting.

In this context, we reported a universal approach to supercharge proteins by noncovalent tagging (Figure 1A). The tag is composed of a cationic arginine8 (R8C) peptide and a Coomassie brilliant blue (CBB) moiety appended on the peptide C-terminus. CBB is a protein-binding dye commonly used in the biochemistry laboratory. It is also an FDA-approved drug under the trade name Brilliant Peel for retinal surgery. Once mixed with proteins, the tag would non-covalently bind to the surface by its CBB moiety and render the protein supercharged. The cationic CPP has been previously used for intracellular protein delivery by non-covalent complexation.[28,30] However, these CPPs and proteins were associated together by electrostatic or hydrophobic interactions, which always leads to nanoparticlization.[31] The tagging strategy yields the supercharged protein in a monodisperse state, which well resembles the naturally occurring and surface-mutated proteins. Moreover, the protein noncovalently tagged by CBB-R8 tags was believed to penetrate cells through membrane permeation, followed by

https://doi.org/10.1021/acs.molpharmaceut.6c00191
Mol. Pharmaceutics 2026, 23, 3722−3731

Downloaded from pubs.acs.org/mpohbp/article-pdf/23/7/3722/6537496/acs.molpharmaceut.6c00191.pdf by WUHAN UNIV user on 20 September 2026

protein-tag dissociation. The cationic tag is likely confined in the anionic plasma membrane, whereas proteins can slip into the cytosol in their native state. Our study demonstrated that the tagging mode is gentler and more efficient than the supercharged +36GFP in cytosolic delivery. With this tag, many proteins, independent of size and pI values, can be supercharged and delivered intracellularly for biological manipulation.

MATERIALS AND METHODS

General

All chemicals and solvents were purchased from commercial source (Bidepharm, and others) and used directly as received without further purification unless otherwise noted. The CCK8 cytotoxicity assay kit and BCA protein assay kit were obtained from Beyotime Biotechnology. Cytochrome C and saporin were obtained from Sigma Aldrich. Flash column chromatography was performed with silica gel (200−300 mesh) purchased from Accela ChemBio. Mass spectroscopy was performed using an LCQ Fleet Ion Trap Mass Spectrometer (Thermo Fisher Scientific) in the Mass Spectrometry Center, School of Pharmaceutical Sciences, Wuhan University.

Synthesis of Compound 1. To 20 mL of phosphorus oxychloride at 0 °C, CBB (3.00 g, 3.61 mmol) was added. The suspension was allowed to warm to room temperature and then stirred for 2 h under a nitrogen atmosphere. Reaction progress was monitored by TLC (DCM/MeOH = 10:1), which showed the formation of a new spot upside the starting material CBB. Upon completion, the mixture was slowly poured into ice-cold water (200 mL). The resulting precipitate was collected by filtration and dried under reduced pressure to afford the crude product 1 as a blue solid (1.08 g, 1.27 mmol, 35% yield). The product was directly used in the next step without purification. MS (ESI): m/z calculated for $C_{47}H_{48}ClN_3O_6S_2$ $[M + H]^+$ 850.27, found 850.28.

Synthesis of Compound 2. *N*-(2-Aminoethyl) maleimide hydrochloride (0.21 g, 1.50 mmol) was added into 50 mL of DCM and cooled to 0 °C. To the mixture, 1 g of compound 1 (1.18 mmol) was slowly added, followed by a supplement of DIPEA (0.5 mL, 3.50 mmol). The reaction was then stirred at room temperature for 2 h. After being stopped by water (40 mL), the reaction was extracted with EtOAc (40 mL × 2). The combined organic layers were washed with 10% aqueous citric acid solution (50 mL) and brine (50 mL). The organic phase was dried with Na_2SO_4, filtered, and concentrated in vacuo. The residue was purified by silica gel column chromatography (DCM: MeOH = 20:1−10:1, v/v) to provide the product 2 as a blue solid (0.79 g, 0.83 mmol, 71%). ^{1}H NMR (600 MHz, DMSO-d_6): δ 10.08 (s, 1H), 9.90 (s, 1H), 7.88 (t, J = 6.4 Hz, 1H), 7.84−7.78 (m, 1H), 7.72 (d, J = 8.2 Hz, 1H), 7.65 (d, J = 7.9 Hz, 1H), 7.62 (d, J = 2.0 Hz, 1H), 7.59−7.56 (m, 1H), 7.54−7.50 (m, 2H), 7.49 (d, J = 7.7 Hz, 1H), 7.43 (d, J = 8.2 Hz, 1H), 7.32 (t, J = 7.8 Hz, 1H), 7.24 (d, J = 8.9 Hz, 2H), 7.19 (t, J = 8.0 Hz, 3H), 7.03 (d, J = 8.9 Hz, 2H), 6.99 (d, J = 8.8 Hz, 2H), 6.96 (d, J = 3.2 Hz, 2H), 6.93 (s, 1H), 6.87 (s, 1H), 6.84 (s, 1H), 6.81 (d, J = 8.5 Hz, 1H), 6.78 (d, J = 9.1 Hz, 1H), 6.66−6.61 (m, 1H), 4.88 (s, 2H), 4.81 (s, 2H), 4.04 (d, J = 7.0 Hz, 2H), 3.65 (d, J = 7.3 Hz, 2H), 3.40 (s, 2H), 2.89 (d, J = 6.3 Hz, 2H), 1.78 (s, 3H), 1.34 (t, J = 6.9 Hz, 3H), 1.21 (t, J = 7.0 Hz, 6H). MS (ESI): m/z calculated for $C_{53}H_{55}N_5O_8S_2$ $[M + H]^+$ 954.3565, found 954.3570.

Compound 3 Synthesis and Purification. At room temperature, NH_2-RRRRRRRRC−CO_2H (5 mg, 0.004 mmol) was dissolved in 1 mL of PBS buffer (137 mM NaCl, 2.7 mM KCl, 10 mM Na_2HPO_4, and 1.8 mM KH_2PO_4, pH 7.4) and transferred to a centrifuge tube. Then, compound 2 (6.5 mg, 0.007 mmol) was dissolved in 0.3 mL of DMF and added into the tube. The mixture in the tubes was gently agitated at room temperature for 1 h. The reaction mixture was then applied to a C18 column and purified by a Biotage flash chromatography system. The fraction containing the product peak was concentrated in a SpeedVac lyophilizer to obtain compound 3 (5.3 mg) in a yield of 63%. The tag compound was >95% pure by HPLC analysis. MS (ESI): m/z calculated for $C_{104}H_{158}N_{38}O_{18}S_3$ $[M+3H]^{3+}$ 775.4004, found 775.4018; $[M+4H]^{4+}$ 581.8023, found 581.8034; $[M+5H]^{5+}$ 465.6434, found 465.6449; $[M+6H]^{6+}$ 388.2041, found 388.2063.

Protein Expression and Purification. All the recombinant proteins were expressed in the *E. coli* bacterial system and purified by the nickel-NTA (nickel-nitrilotriacetic acid) affinity chromatography. Take +36GFP for example, the pET29 vector bearing the +36GFP and 6xHis tag insert was purchased from Addgene (Plasmid # 62937). The vector was transformed into *E. coli* Rosetta 2(DE3) cells (Millipore, USA). The strain was grown in Luria−Bertani medium until OD600 reached at 0.6 to 0.8. Isopropyl β-D-thiogalactoside (IPTG) was added to the medium at a final concentration of 1 mM. 4 hours later, the culture was harvested and resuspended in lysis buffer (20 mM Tris−HCl, pH 7.2, 0.3 M NaCl). The bacteria suspension was lysed by French press and centrifuged at 12000g for 10 min. The His × 6 tagged protein was purified from the supernatant by Ni affinity chromatography, followed by the ion exchange chromatography equipped with HiScreen SP HP (Cytiva) column. The purified protein was then exchanged to PBS by the Sephadex G-25 desalting column and stored at −30 °C in the presence of 10% glycerol for later use.

The expression vectors encoding GFP (plasmid #85492), Cre recombinase (plasmid #62939), Nano luciferase (plasmid #141289), and pCMV-DeAct-GS1 (plasmid #89445) were all obtained from Addgene. Proteins were expressed and purified using a similar procedure aforementioned. The purified proteins were characterized by SDS-PAGE (Figure S1) and stored at −30 °C in the presence of 10% glycerol.

Zeta Potential. For zeta-potential measurements, the tagged protein (1 mg/mL in PBS, pH 7.4, with tagging ratios from 3/1 to 20/1) were diluted 10 times in Milli-Q water, and 700 μL of the diluted sample was loaded in a disposable folded capillary cuvette (DTS1070, Malvern Panalytical). Three measurements were performed by Zetasizer Nano ZS (Malvern Panalytical) at intervals of 300 s, and each measurement comprised 20 runs.

Cell Culture Condition. MDA-MB-231, HEK-293T, CHO−K1, ARPE-19, Jurkat, HeLa, and NIH-3T3 cell lines were obtained from the American Type Culture (ATCC) and maintained in Roswell Park Memorial Institute (RPMI) 1640 medium supplemented with 10% fetal bovine serum (FBS) and 1% penicillin/streptomycin. RPMI 1640 medium, FBS, and other cell culture supplementary reagents were purchased from Procell Inc. (Wuhan, China). All the cell lines were propagated in a humidified incubator at 37 °C with 5% CO_2.

Protein Tagging and Intracellular Delivery. Purified tag 3 was dissolved in water to reach a stock concentration of 1 mM and stored at −20 °C. To tag proteins, tag solution was mixed with a protein solution in PBS (25 μM) at the indicated tagging ratio (3/1−20/1). The mixture was incubated at 37 °C in a water bath for 20 min and then stored at 4 °C until use. The tagged protein has to be used in less than 1 day after preparation, owing to the instability of some proteins. To deliver proteins, cell monolayer (24-well plate) was washed once with serum-free RPMI1640 and treated with 500 μL of RPMI1640 containing the indicated concentrations of tagged proteins (0.05, 0.1, 0.15, 0.25, 0.5, and 1 μM). Cells were returned to the 37 °C cell incubator and cultured for another 4 h otherwise indicated. The cell monolayer was then washed twice by ice-cold RPMI1640, and it became ready for next-step analysis.

Microscopic Imaging and Quantification. The fluorescent images of treated cells were captured by an Olympus IX73 microscope fitted with a plan apochromat object 40×. Filter cubes U-FBNA (BP470−495, BA510−550) and TEXRED (ET560/40x, ET630/75m) were used for GFP and dsRed imaging, respectively. To trace the intracellular distribution, a Zeiss LSM 700 confocal microscope was used for imaging. GFP and AF594 were excited with a 488 nm argon ion laser or 594 nm laser lines, respectively. The fluorescence was recorded through frame scan. The fluorescent intensity in cytosol was quantified by measuring the pixel intensity using ImageJ 1.54p software. The mean fluorescent intensity (MFI) of cells was measured

Downloaded from pubs.acs.org/mpohbp/article-pdf/23/7/3722/6537496/7/acs.molpharmaceut.6c00191.pdf by WUHAN UNIV user on 20 September 2026

https://doi.org/10.1021/acs.molpharmaceut.6c00191
Mol. Pharmaceutics 2026, 23, 3722−3731

by CytoFLEX S flow cytometry (Beckman Coulter) and analyzed by FlowJo V10.

Protein Labeling by AF594. To visualize the intracellular distribution, aprotinin, cytochrome C, BSA, and human IgG were labeled by Alexa Fluor 594 (AF594) NHS ester. Briefly, proteins were dissolved in PBS buffer at a concentration of 6 mg/mL. To the protein solution (100 μL), AF594-NHS dye (Duofluor) was added by a dye/protein ratio of 3/1. The labeling reaction was gently mixed at room temperature for 5 h, followed by purification on G-15 desalting column (Cytiva) to remove free dye molecules. The purified protein was measured by BCA assay and stored at −30 °C in the presence of 10% glycerol for later use.

Time-Lapse Imaging Uptake in Live Cells. Time-lapse images were captured every 60 s on an inverted OXFORD Andor BC43 benchtop microscope equipped with a stage-top incubation and humidified with 5% CO_2 at 37 °C. Before imaging, cell monolayer (MDA-MB-231 cell) was washed once with RPMI 1640 and added with 1 mL of serum-free media containing 250 nM of tagged GFP (tag/GFP ratio 10/1). Cells were immediately imaged and traced by the fluorescent microscopy.

Cell Fractionation and Nluc Assay. Cell monolayers (MDA-MB-231) in a 24-well plate were treated with 250 nM of the tagged Nluc (tagging ratio 5/1, 10/1, or 15/1) at 37 °C for indicated time intervals (0.5 h, 1 h, 2 h, 4 h, or 6 h). Cells were washed twice by cold RPMI1640 and collected in 300 μL of homogenization buffer (TEA 250 buffer, consisting of 10 mM triethanolamine, 1 mM EDTA, 250 mM sucrose, 10 mM acetic acid, pH 7.4). Homogenization was performed by passing cell suspension through narrow-gauge needle (31G) 20 times until all cells were lysed and stainable by Trypan blue. The lysate was subjected to high-speed centrifugation (225000g for 1.5 h) to carefully separate the supernatant (containing cytosol) from the pellet (containing membrane and organelles). The pellet was resuspended in 500 μL of homogenization buffer containing 0.1% SDS. 10 μL of the aliquots from the supernatant and pellet suspension was transferred to the 96-well plate and applied with the Nano-Glo luciferase assay substrate (Promega). The signal was quantified by an Infinite M Plex microplate reader (Tecan) and plotted against the tagging ratio or concentration using GraphPad Prim 9.3.

Endocytosis Inhibition Assay. MDA-MB-231 cells were pretreated with RPMI 1640 media containing NaN_3 (7 mM), CPZ (5 μM), NH_4Cl (50 mM), Dynasore (5 μM), EIPA (5 μM), and chloroquine (25 μM) for 0.5 h 37 °C. The cells treated by blank RPMI1640 media at 37 and 4 °C were used as negative and positive control, respectively. Cells were then added with the tagged Nluc (250 nM) and incubated for another 4 h. The cell monolayer was washed twice by cold RPMI1640 and lyzed for cell fractionation aforementioned. The Nluc concentrations in cytosol and organelle fractions were quantified by luciferase assay, respectively. The inhibitory effect was assessed by comparing with the untreated cells (negative control).

In Vitro Cre Delivery and Recombination. The reporter plasmid pCALNL-dsRed was purchased from Addgene (Plasmid #13769). HeLa cells were plated at 40,000 cells per well in 24-well plates 1 day before experiment. pCALNL-DsRed (500 ng) was then transfected into cells using the JetPRIME reagent (Sartorius). After incubation for 4 h in RPMI1640 with tagged Cre protein (250, 500, and 1000 nM), cells were washed three times with 20 U/mL heparin in PBS and incubated in growth medium (5% FBS) for 24 h. The cytosolic Cre delivery, which is associated with DNA recombination and dsRed expression, was analyzed by flow cytometry and fluorescence microscopy.

deAct-GS1 Delivery. NIH-3T3 cells were seeded in the glass-bottom dish and cultured overnight. Cells were washed once by RPMI1640 and treated with 1 mL of serum-free media containing 250 nM of tagged GFP or deAct-GS1 protein (tagging ratio 10/1). 6 hours after incubation, cells were washed twice by cold PBS and fixed in 4% formaldehyde (prepared from paraformaldehyde) for 15 min. The monolayer was then permeabilized with 0.1% Triton X-100 for 3 min and then blocked in 3% BSA in PBS. Phalloidin-AF594 was diluted into 1× working solution and applied on the cells for 20 min at room temperature. Cells were then washed three times to remove the residual dyes and immerged in 300 μL of RPMI1640 for confocal imaging. Actin filaments were visualized via the phalloidin-AF594, and the tagged protein in cytosol, including deAct-GS1, was traced by the GFP fluorescence.

Saporin-Induced Cytotoxicity Assay. MDA-MB-231 cells (5000 cells/well, 5 repeat wells) was seeded in 96-well plates and allowed to attach for 24 h. The cells were treated with saporin alone as the negative control while the tagged saporin (tag/saporin ratio 10/1) as the positive control. A series of protein concentrations (0.03−1.2 μg/mL) were applied and coincubated with cells for 48 h. The viable cells were analyzed by the CCK-8 kit according to the manufacturer's protocol. The cell viability was expressed as a percentage relative to the value of untreated controls (100%).

Statistical Analysis. Statistical analysis was performed using GraphPad Prism 9.3.0, data were presented as mean ± standard deviation, P-values were calculated using the two-way ANOVA with Tukey's multiple comparison test, and $P < 0.05$ was considered to be statistically significant.

RESULTS AND DISCUSSION

Tag Design for Protein Supercharging

Despite the cationic nature, the R8 peptide generally has no or only very weak affinity to proteins. CBB acts as a molecular glue that plays a vital role in the tagging process. It was selected because of its good biosafety, moderate affinity, and compatibility to many proteins for tagging.[32] In its structure, CBB contains two sulfonic acid groups, which both can be used for functionalization. Here, we only selected one group for modification because previous reports revealed that the sulfonic group might participate in the ionic interaction with proteins.[33] To selectively functionalize on one sulfonic group, the chlorination procedure was carefully controlled with the reaction time and temperature (Figure 1B). The monosulfonyl chloride **1** is quite stable, which can be washed with cold water and characterized in the LC−MS spectrometry (Figure S2). The sulfonyl chloride **1** was then reacted with 2-maleimidoethylamine to generate the compound **2** in a good yield (Figure S3). This maleimide-CBB **2** is reactive and readily conjugated with the R8C peptide (NH_2-RRRRRRRRC−CO_2H) to yield the final product tag **3**. The tag compound **3** was purified by high-performance liquid chromatography (HPLC) and confirmed to be >95% purity for biological experiments (Figure S4). The molecular weight and isotopic pattern match the expected value (Figure S5), indicating the successful synthesis of the CBB-R8 tag.

CBB can interact with proteins via the van der Waals force and ionic interaction,[33] which are widely available on most protein surface. The broad distribution of binding pockets on proteins allows the tagging at a variable ratio, indicating an ease control of charge intensity. Using the peptide tag, we first titrated GFP with variable tagging ratios. It was selected as a model protein because the tagged GFP can be compared with the engineered +36GFP, which is a gold standard in the field of supercharged proteins. We first analyzed the tagged GFP by zeta-potential (ζ) determination, as shown in Figure 1C. With the increasing of tagging ratio (tag/GFP), we observed a gradual increment of zeta-potential values from −4.76 mV to 14.5 mV. At the ratio 10/1 (tag/GFP), the tagged GFP has a comparable zeta-potential value (+8.04 mV) to the supercharged +36GFP (+8.26 mV). Considering the high number of tags associated with protein, the tagged GFP might possess more net charges than +36GFP. It is rational, considering the tags can extend outside of GFP and render a larger sphere than

Downloaded from pubs.acs.org/mpohbp/article-pdf/23/7/3722/6537496/7/acs.molpharmaceut.6c00191.pdf by WUHAN UNIV user on 20 September 2026

https://doi.org/10.1021/acs.molpharmaceut.6c00191
Mol. Pharmaceutics 2026, 23, 3722−3731

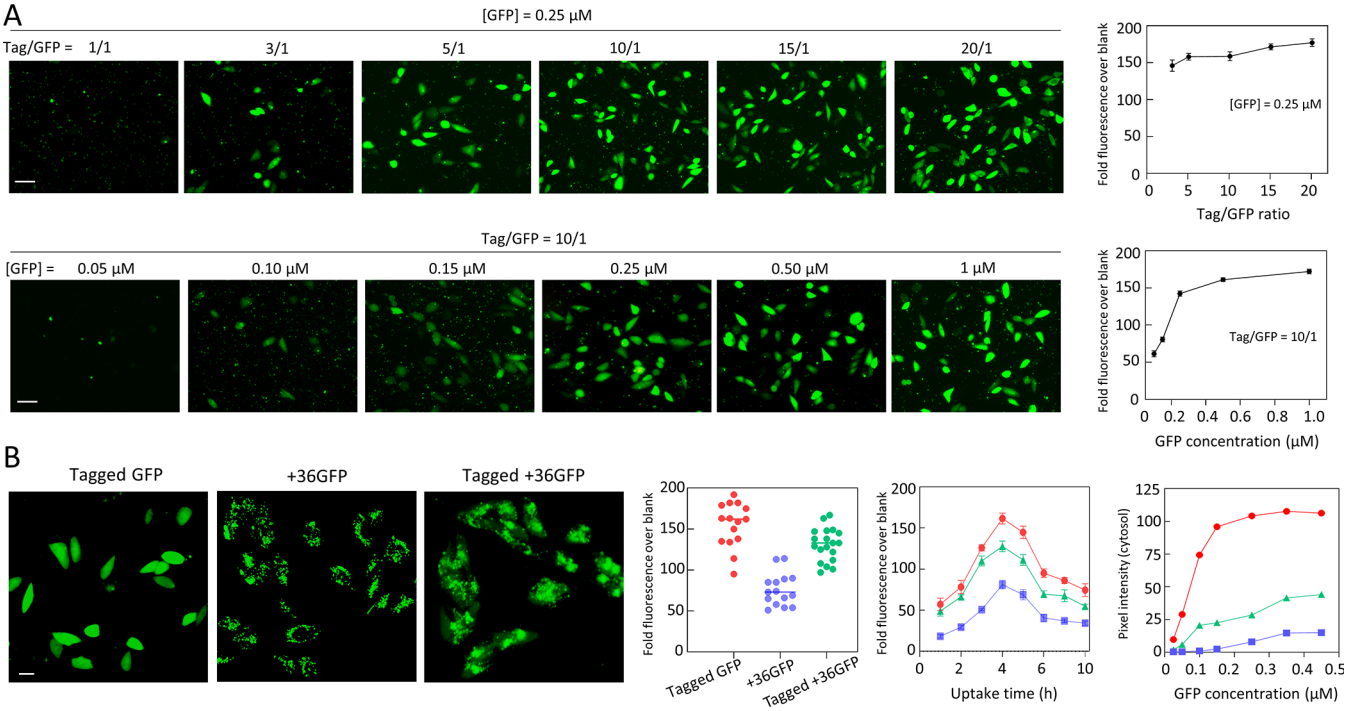

Figure 2. Impact of tagging conditions on the GFP delivery to MDA-MB-231 cells. (A) The cytosolic delivery is minimally affected by the tagging ratio but dramatically enhanced by the higher concentration of GFP. Scale bar, 30 μm. (B) Comparison of the delivery effect by the tagged GFP, +36GFP, and the combined mode. The semiquantitative analysis of the cytosolic signal over uptake time and GFP concentrations is showed on the right panels. Scale bar, 10 μm.

the surface-mutated +36GFP, which could accommodate more charges (Figure 1D). Despite the super cationic feature, the tagged GFP is biocompatible and exhibits little toxicity in the cell viability assay (Figure S6).

Intracellular Delivery of Supercharged GFP and Other Proteins

After characterization, we set out to evaluate the capability of the cytosolic delivery of the tagged GFP. The cell fluorescence was imaged after 4 h treatment by supercharged GFP of different tagging ratios. As shown in Figure 2A, we found that the tagging ratio has a significant impact on the degree of the cellular uptake. A plateau was reached at a ratio as low as 3/1 (tag/GFP). Meanwhile, the GFP concentration also affects the delivery efficiency but mainly impacts the intracellular fluorescent intensity rather than the proportion of GFP-positive cells. Next, we compared the ability of the tagged GFP, +36GFP, and the tagged +36GFP to penetrate mammalian cells and reach the cytosol. As shown in Figure 2B, all three proteins could be taken up by cells but exhibited different intracellular distribution models. Cells treated by the tagged GFP showed a homogeneous fluorescence distribution, suggestive of the cytosolic location of GFP proteins. In contrast, the +36GFP displays a spot pattern, which is in agreement with the previous report that multiple pathways are involved in the uptake mechanism of +36GFP.[34] In the tagged +36GFP group, we saw a mixed pattern, indicating an additive effect on delivery. It is noted that the tagged GFP, albeit more cationic than +36GFP, shows a heterogeneous uptake in comparison to +36GFP groups. Nearly 40% of cells are dim in green fluorescence, while cells treated by +36GFP have the homogeneous population in flow cytometric plots (Figure S7).

Interestingly, a strong accumulation in the nuclei was observed in cells treated with +36GFP. To better visualize the phenomenon, we analyzed the intracellular distribution of +36GFP by confocal imaging and colocalized it with the nucleus. As shown in Figure S8, we confirmed the much higher intensity of the GFP signal in the nuclear envelope by counterstaining nuclear membrane protein Lamin B1 with immunofluorescence. This observation might be attributed to the nucleus-tropic nature of cationic proteins.[29] This nucleus-tropic phenomenon has not been seen in the tagged GFP group, where we used the canonical GFP (charge-neutral). The observation indicates that the cationic tags have already dissociated from GFP in the cytosol, otherwise it could be seen in the nucleus. The observation indicates that the cationic tags have already dissociated from GFP in the cytosol, but its presence in cells only lasts for around 4 h and then gradually diminishes (Figure 2B), likely due to the intracellular degradation by proteasomes.[35]

The cytosolic delivery of tagged GFP was then expanded to more cell lines, as shown in Figure 3A. All the tested cell lines, including MDA-MB-231, HEK-293T, CHO−K1, APRE-19, and the difficult-to-transfect Jurkat cells, showed a profound intracellular delivery efficiency. The exciting results encouraged us to expand the tagging strategy toward more proteins: aprotinin, cytochrome C, BSA, and IgG, ranging from 6.5 kDa to 150 kDa. The CBB-R8 tag can supercharge all proteins but yields different charge intensities and ζ-potentials (Figure 3B). For example, aprotinin is the smallest but obtained a ζ-potential value as high as +15.3 mV (ratio = 20/1). IgG is larger, but on the contrary, it can be only charged to +8.81 mV. Accordingly, the remarkable delivery efficiency has been observed by all these tagged proteins, with the exception of IgG. Its distribution in cells is shown as spots, suggestive of the endosomal entrapment. The low efficiency associated with IgG is likely attributed to the lower charging potential of IgG,

Downloaded from pubs.acs.org/mpohbp/article-pdf/23/7/3722/6537496/acs.molpharmaceut.6c00191.pdf by WUHAN UNIV user on 20 September 2026

https://doi.org/10.1021/acs.molpharmaceut.6c00191
Mol. Pharmaceutics 2026, 23, 3722−3731

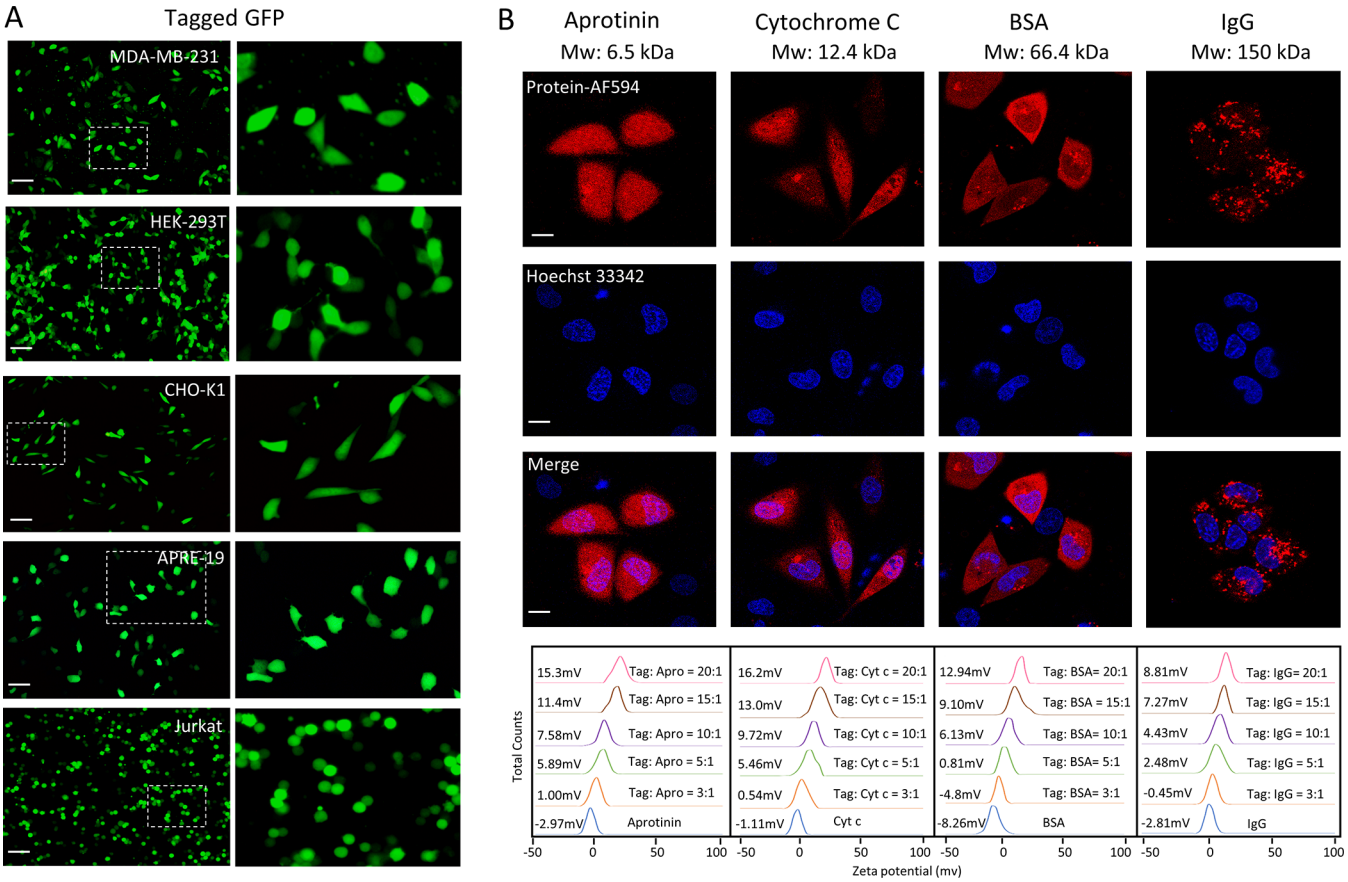

Figure 3. Validation of the cytosolic delivery effect across cell lines and protein cargoes. (A) GFP delivery in 5 cell lines, including adhesive tumor cells (MDA-MB-231), normal cells (HEK-293, ARPE-19 and CHO−K1), and suspension cells (Jurkat). The regions of dashed squares are zoomed in and shown on the right. Scale bar, 50 μm. (B) Confocal images of MDA-MB-231 cells to show the cytosolic delivery of AF594-labeled aprotinin (6.5 kDa), cytochrome C (12.4 kDa), BSA (66.4 kDa), and IgG (150 kDa) by tagging (ratio 10/1). The zeta-potential status of these proteins after tagging is shown below. Scale bar, 10 μm.

which indicates a limitation of this supercharging strategy. The reason is not entirely clear but it might be related to the amino acid sequence and the protein topology. When the CBB dye binds to protein molecules, it interacts chiefly with arginine residues, although it also interacts avidly with histidine, lysine, and tyrosine.[36] The bias of CBB to residues may render a variation of the charging potential to different proteins, which attenuates the universalizability of this technology.

It is worth noting that the protein supercharging and intracellular delivery were all performed under serum-free conditions. The interaction between GFP and the CBB moiety of tags is reversible and could be interrupted by the competition from other proteins, for example, BSA in serum (Figure S9). However, it would not affect its application in local drug delivery because the tag could supercharge and deliver proteins to the target cells in vivo without the involvement of systemic circulation.

Supercharging through the Plasma Membrane Is Largely Independent of Endocytosis

To illustrate the uptake mechanism of the tagged proteins, we traced the cell uptake process by time-lapse microscopy. A gradual increase in the diffuse GFP fluorescence was observed in the cytosol (Figure 4A). The clear presence of cytosolic GFP was seen as early as 60 s after the supercharged GFP was applied to cells, and the fluorescence intensity continued to increase until the end point of the experiment (6 min). There is no punctate spot appearing during the whole process, suggestive of the absence of endosomal uptake. The result is in line with other studies reporting direct cytosolic delivery.[37,38]

To further confirm the nonendocytic pathway, we tried to quantify the efficiency by delivering the reporter protein Nano luciferase (NLuc). NLuc is a luciferase enzyme (19.1 kDa) that produces a high-intensity glow-type bioluminescence.[39] It is a highly sensitive tracer and could be detected by a concentration as low as 0.01 pM in vitro.[40,41] In this study, Nluc was supercharged by tagging and applied to cell monolayers for uptake. Cells were then ruptured by 20 passages through a 31G needle and centrifuged at high speed (225,000g) for 1.5 h to obtain cytosolic (supernatant) and organelle/membrane fractions (pellet), respectively.[42] The Nluc in the fractions was analyzed and compared. As shown in Figure 4B, the cytosolic Nluc accounts for the majority (>80%) of cargo protein uptake by cells in all conditions we tested (different tagging ratios and uptake times).

We next investigated the uptake mechanism by pretreating cells with small-molecule inhibitors, as listed in Figure 4C. The most common endocytosis inhibitors, including NaN_3, chlorpromazine (CPZ), dynasore (Dyn), ethylisopropylamiloride (EIPA), and chloroquine (CQ), have a minor impact on the cytosolic delivery of tagged Nluc. However, exposure to ammonium chloride (NH_4Cl) can suppress the cellular uptake of Nluc protein. As a weak base, extracellularly applied ammonium chloride is able to diffuse across the cell membrane

https://doi.org/10.1021/acs.molpharmaceut.6c00191
Mol. Pharmaceutics 2026, 23, 3722−3731

Downloaded from pubs.acs.org/mpohbp/article-pdf/23/7/3722/6537496/acs.molpharmaceut.6c00191.pdf by WUHAN UNIV user on 20 September 2026

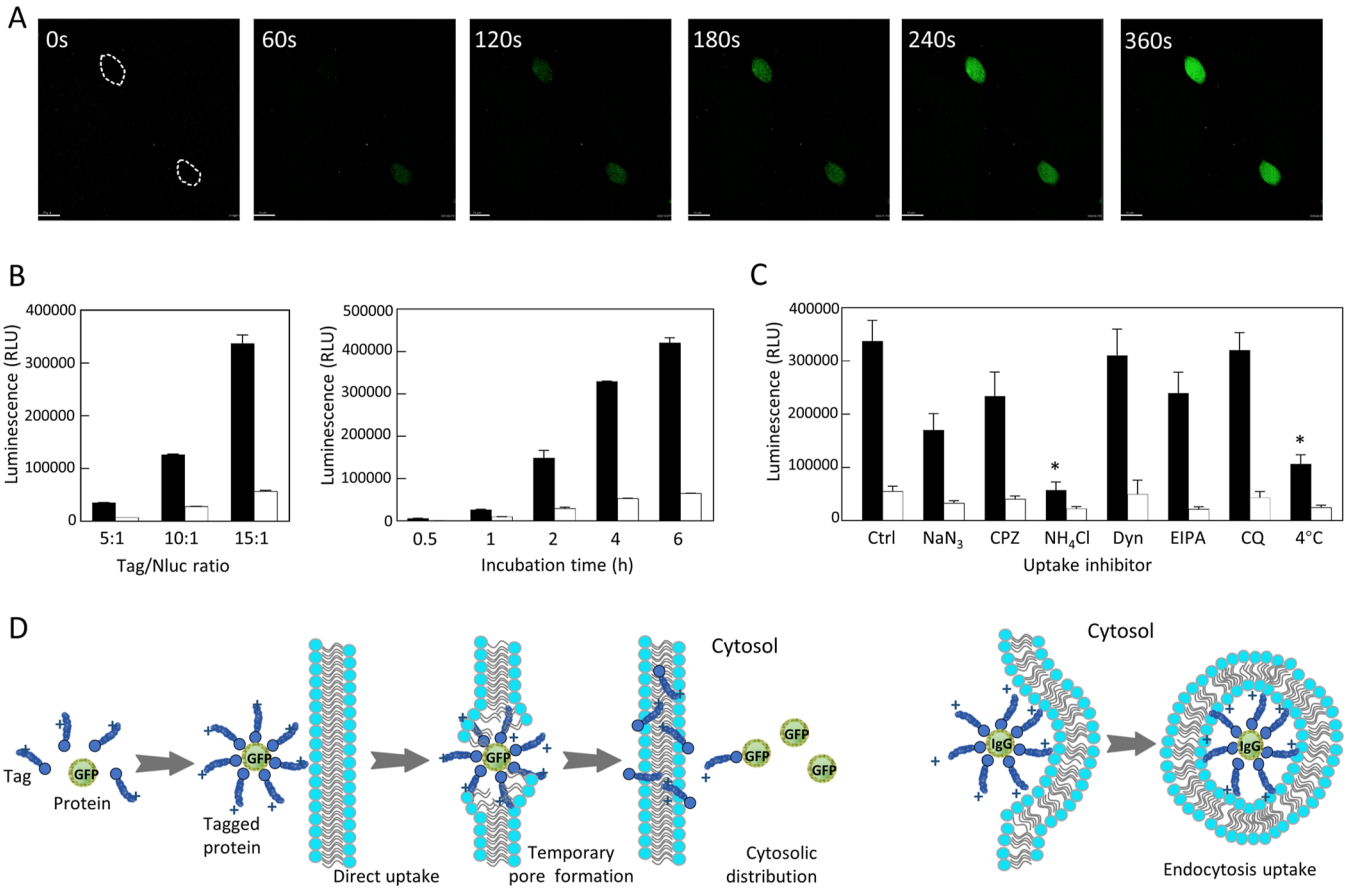

Figure 4. Mechanism study of the cytosolic delivery mediated by tagged proteins. (A) Images of time-lapse confocal microscopy revealing the direct membrane penetration by the tagged GFP. Scale bar, 10 μm. (B) The uptake intensity (but not efficiency) is affected by the tagging ratio (left panel) and incubation time (right panel). (C) Cells were pretreated with the indicated inhibitors to assess the uptake pathway of the tagged reporter protein Nluc. Ctrl, control group without inhibitors; CPZ, chlorpromazine; Dyn, dynasore; EIPA, ethylisopropylamiloride; CQ, chloroquine. The concentrations of inhibitors: NaN_3 (7 mM), CPZ (5 μM), NH_4Cl (50 mM), dynasore (5 μM), EIPA (5 μM), chloroquine (25 μM). *, $P < 0.05$. The reporter signals in cell fractions were shown in the black-filled (cytosol) and white-filled (membrane and organelles) histograms, respectively. (D A proposed mechanism of membrane penetration via temporary pore formation and subsequent electrostatic shedding of tags. The endocytic uptake of IgG is illustrated on the right for comparison.

in its uncharged ammonia (NH_3) form and sequester protons in endosomes, thus raising the endosomal pH. The pH alteration can significantly inhibit the activity of acid-dependent enzymes in endosomes, making NH_4Cl a well-known inhibitor of endocytosis. It is interesting that ammonium chloride also has a strong inhibitory effect on the cytosolic entry of tagged proteins, which we proved to be independent of endocytic pathways. A recent study by Lazarenko revealed that extracellularly applied ammonium chloride could also alkalize the cytosol of nerve cells. The intracellular alkalinization causes an intracellular Ca^{2+} increase and subsequent membrane depolarization.[43] A similar observation on rat hepatocytes and other cells has also been reported in several independent studies, albeit with slightly different mechanism interpretations.[44,45] We speculated that the intracellular alkalinization causes depolarization and decreases negative charges in the inner leaflet of plasma membrane, which attenuates the electrostatic interaction with the tagged and supercharged Nluc. At the same time, we found that dropping the incubation temperature could reduce cytosolic delivery. This is because the low temperature decreases the membrane fluidity and the corresponding penetration.[46] However, a significant drop of uptake at lower temperatures indicates that the energy-dependent endocytosis, such as macropinocytosis, might contribute to the uptake of tagged Nluc as well. It is in agreement with the observation in flow cytometric experiments that treatments by NaN_3 and EIPA have impacts on the cellular uptake of tagged GFP (Figure S10). All together, these results demonstrated that membrane penetration plays the major role, and cell entry by protein supercharging can largely avoid the endocytic pathway.

On the basis of these results, we may propose a mechanism to explain the direct membrane penetration of the tagged protein. As shown in Figure 4D, the tagging process supercharges the GFP protein surface and initiates an interaction with the anionic cell membrane. This may lead to temporary pore formation and subsequent entry of GFP inside the cytosol. The performance of this entry has also been observed within the direct membrane penetration of amphiphilic molecule-coated nanoparticles.[47] Inspired from this study from the Prof. Jana group, we may speculate that the weak and modular interaction between protein and tags plays a vital role in the cytosolic delivery. The reversibility of the tagging model separates the interaction with the cell membrane and their cytosolic entry, making the membrane penetration straightforward and energy-independent. Meanwhile, the feasibility of pore formation may vary depending on the size of proteins, as the tagged IgG, which is larger in

https://doi.org/10.1021/acs.molpharmaceut.6c00191
Mol. Pharmaceutics 2026, 23, 3722−3731

Downloaded from pubs.acs.org/mpohbp/article-pdf/23/7/3722/6537496/acs.molpharmaceut.6c00191.pdf by WUHAN UNIV user on 20 September 2026

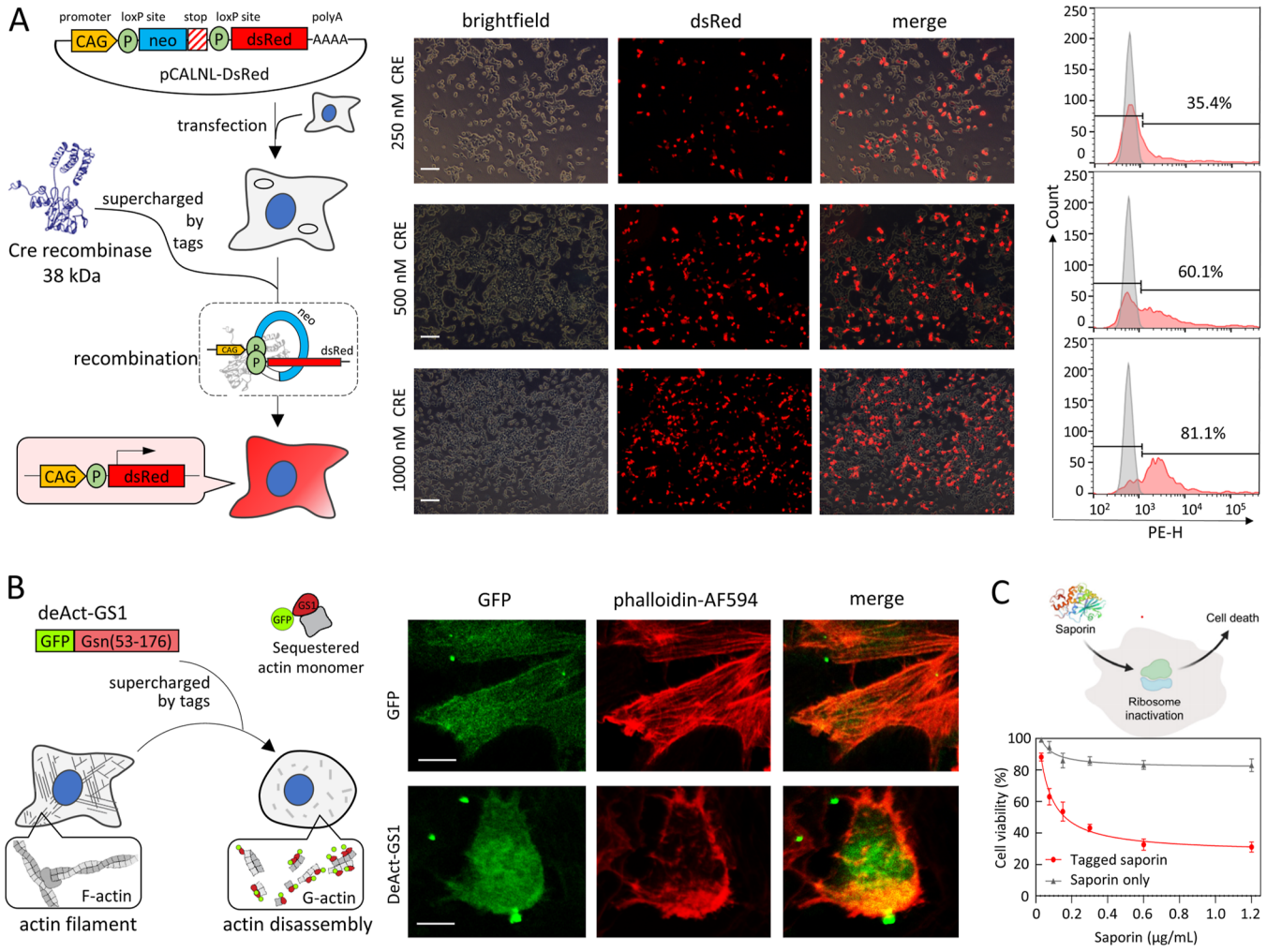

Figure 5. Delivery of active proteins to the cytosol for biological manipulation. (A) Delivery of Cre recombinase to the cytosol for Cre-loxP recombination and dsRed expression in HeLa cells. The dsRed cassette was transiently transfected into cells using JetPRIME before the experiment. The images are the overlay of dsRed signal and brightfield cells. The percentage of positive cells was quantified by flow cytometry and compared with the untreated blank cells (gray filled histograms). Scale bar, 50 μm. (B) The tagged deAct-GS1 protein was delivered into NIH-3T3 cells to disassemble the actin filament, which consequently alters cell morphology. Scale bar, 10 μm. (C) Intracellular delivery of saporin by tags results in ribosomal inactivation and cell death. MDA-MB-231 cells treated by the saporin only are less affected.

molecular size, is taken up by cells mainly via endocytic pathways.

Tagged Protein Is Discharged and Functional in the Cytosol

Next, we proceeded to prove that the protein after cytosolic delivery remains biologically functional. We first tried to deliver an enzyme, Cre recombinase, to mammalian cells. Cre recombinase is a 38 kDa topoisomerase that catalyzes the site-specific recombination of DNA between loxP sites.[48] After transient transfection of pCALNL-dsRed (a dsRed-based Cre activity reporter) plasmid,[49] we supercharged Cre and tested its ability of DNA recombination in HeLa cells. The function of delivered Cre was assessed by monitoring dsRed expression using fluorescence microscopy and flow cytometry (Figure 5A). We observed a dose-dependent recombination activity after Cre delivery by tags. The recombinant cells could account for over 80% when 1 μM Cre was applied. This percentage is quite high if we take into account the impact of pCALNL-dsRed transfection efficiency.

Functional delivery was further evaluated in fibroblast cells NIH-3T3 using deACT-GS1 protein as cargo (42 kDa). Gelsolin segment 1 (GS1) is a ~120-amino-acid domain that can sequester actin monomers and disrupt actin filaments. DeAct-GS1 is a GFP fusion protein designed by the Zuchero lab to manipulate and monitor actin dynamics in eukaryotic cells.[50] When the tagged deAct-GS1 was delivered into the cytosol, the functional cargo would disassemble the actin filament (F-actin) and cause the loss of the flattened cell morphology, as seen in Figure 5B. As a comparison, the control cargo GFP could also been delivered into the cytosol, but the treated cells retain the network of actin filaments, as stained by phalloidin-AF594. The result demonstrated that the cytosolic deACT-GS1, delivered by tagging and supercharging, is functional to sequestrate actin filaments inside cells.

We also explored the direct cytosolic delivery of toxic proteins by using the tagging method. Saporin is a plant-derived ribosome-inactivating protein (28.6 kDa). It is membrane-impermeable and has to reach the cytosol to elicit its cytotoxicity. Figure 5C shows the viability of MDA-MB-231 cells treated by the saporin alone or tagged by the CBB-R8 tag. The supercharged saporin exhibited a significantly improved antiproliferation effect than the naked saporin, which is in line

Downloaded from pubs.acs.org/mpohbp/article-pdf/23/7/3722/6537496/acs.molpharmaceut.6c00191.pdf by WUHAN UNIV user on 20 September 2026

https://doi.org/10.1021/acs.molpharmaceut.6c00191
Mol. Pharmaceutics 2026, 23, 3722−3731

with the direct cytosolic delivery and observation of the above two proteins. These results collectively indicated that the supercharging strategy described in this work is not unique to a specific protein or a single application but instead is broadly useful in biological sciences.

CONCLUSIONS

In summary, we harnessed the pan-protein binding ability of CBB to design a tag that can supercharge proteins for cytosolic delivery. By side-by-side comparisons of the tagged GFP and the supercharged +36GFP, we demonstrated that the tagging approach results in a higher level of charge density and a significantly greater efficiency of cytosolic delivery. Moreover, reversibility of the tagging process enables proteins to be discharged once inside cells, showing advantages such as an even distribution, less interruption to protein functions, and universal potential for broad applications. Aided by tagging and supercharging, functional Cre recombinase, deAct-GS1, and saporin proteins can be delivered to cells and elicit biological functions. This study collectively demonstrates the potential of the tagging approach on protein supercharging and cytosolic delivery, which may help expand protein therapeutics to more intracellular targets.

ASSOCIATED CONTENT

Data Availability Statement

All the data and experimental parameters related to this paper are available in the main text and the material and methods section.

Supporting Information

The Supporting Information is available free of charge at https://pubs.acs.org/doi/10.1021/acs.molpharmaceut.6c00191.

HPLC and mass spectra of compounds, cell viability data, confocal images, flow cytometry plots, and SDS-PAGE gel images (PDF)

AUTHOR INFORMATION

Corresponding Author

Wanyi Tai − *Department of Pharmaceutical Engineering, School of Pharmaceutical Sciences, Wuhan University, Wuhan 430071 Hubei, China;* orcid.org/0000-0003-3589-8263; Email: wanyi-tai@whu.edu.cn

Authors

Yanan Quan − *Department of Pharmaceutical Engineering, School of Pharmaceutical Sciences, Wuhan University, Wuhan 430071 Hubei, China*

Weina Jing − *Department of Pharmaceutical Engineering, School of Pharmaceutical Sciences, Wuhan University, Wuhan 430071 Hubei, China*

Lei Peng − *Department of Pharmaceutical Engineering, School of Pharmaceutical Sciences, Wuhan University, Wuhan 430071 Hubei, China*

Wanrong Yang − *Department of Pharmaceutical Engineering, School of Pharmaceutical Sciences, Wuhan University, Wuhan 430071 Hubei, China*

Complete contact information is available at: https://pubs.acs.org/10.1021/acs.molpharmaceut.6c00191

Notes

The authors declare no competing financial interest.

ACKNOWLEDGMENTS

This work was financially supported by the National Key R&D Program of China (Grant No. 2021YFA0909900) and the National Natural Science Foundation of China (Grant No. 82273860).

REFERENCES

(1) Ma, C.; Malessa, A.; Boersma, A. J.; Liu, K.; Herrmann, A. Supercharged Proteins and Polypeptides. *Adv. Mater.* **2020**, *32* (20), No. e1905309.

(2) Wang, L.; Geng, J.; Wang, H. Emerging Landscape of Supercharged Proteins and Peptides for Drug Delivery. *ACS Pharmacol. Transl. Sci.* **2024**, *7* (3), 614−629.

(3) Simon, A. J.; Zhou, Y.; Ramasubramani, V.; Glaser, J.; Pothukuchy, A.; Gollihar, J.; Gerberich, J. C.; Leggere, J. C.; Morrow, B. R.; Jung, C.; et al. Supercharging enables organized assembly of synthetic biomolecules. *Nat. Chem.* **2019**, *11* (3), 204−212.

(4) Baumer, K. M.; Cook, C. D.; Zahler, C. T.; Beard, A. A.; Chen, Z.; Koone, J. C.; Dashnaw, C. M.; Villacob, R. A.; Solouki, T.; Wood, J. L.; et al. Supercharging Prions via Amyloid-Selective Lysine Acetylation. *Angew. Chem. Int. Ed.* **2021**, *60* (27), 15069−15079.

(5) Simeonov, P.; Berger-Hoffmann, R.; Hoffmann, R.; Sträter, N.; Zuchner, T. Surface supercharged human enteropeptidase light chain shows improved solubility and refolding yield. *Protein Eng. Des. Sel.* **2011**, *24* (3), 261−268.

(6) Prasse, A. A.; Zauner, T.; Büttner, K.; Hoffmann, R.; Zuchner, T. Improvement of an antibody-enzyme coupling yield by enzyme surface supercharging. *BMC Biotechnol.* **2014**, *14*, 88.

(7) Laber, J. R.; Dear, B. J.; Martins, M. L.; Jackson, D. E.; DiVenere, A.; Gollihar, J. D.; Ellington, A. D.; Truskett, T. M.; Johnston, K. P.; Maynard, J. A. Charge Shielding Prevents Aggregation of Supercharged GFP Variants at High Protein Concentration. *Mol. Pharmaceutics* **2017**, *14* (10), 3269−3280.

(8) Vahabpour, R.; Basimi, P.; Roohvand, F.; Asadi, H.; Irani, G. M.; Zabihollahi, R.; Bolhassani, A. Anti-viral Effects of Superpositively Charged Mutant of Green Fluorescent Protein. *Protein Pept. Lett.* **2019**, *26* (12), 930−939.

(9) Simeon, R. L.; Chen, Z. A screen for genetic suppressor elements of hepatitis C virus identifies a supercharged protein inhibitor of viral replication. *PLoS One* **2013**, *8* (12), No. e84022.

(10) Crooks, E. T.; Grimley, S. L.; Cully, M.; Osawa, K.; Dekkers, G.; Saunders, K.; Rämisch, S.; Menis, S.; Schief, W. R.; Doria-Rose, N.; et al. Glycoengineering HIV-1 Env creates 'supercharged' and 'hybrid' glycans to increase neutralizing antibody potency, breadth and saturation. *PLoS Pathog.* **2018**, *14* (5), No. e1007024.

(11) Kronenberg, J.; Britton, D.; Halvorsen, L.; Chu, S.; Kulapurathazhe, M. J.; Chen, J.; Lakshmi, A.; Renfrew, P. D.; Bonneau, R.; Montclare, J. K. Supercharged Phosphotriesterase for improved Paraoxon activity. *Protein Eng. Des. Sel.* **2024**, *37*, gzae015.

(12) Doerr, A. Supercharging through the cell membrane. *Nat. Methods* **2009**, *6* (5), 322.

(13) Thompson, D. B.; Cronican, J. J.; Liu, D. R. Engineering and identifying supercharged proteins for macromolecule delivery into mammalian cells. *Methods Enzymol.* **2012**, *503*, 293−319.

(14) Xie, J.; Xiang, J.; Shen, Y.; Shao, S. Mechanistic Insights into the Tools for Intracellular Protein Delivery. *Chem Bio Eng.* **2025**, *2* (3), 132−155.

(15) Bruce, V. J.; McNaughton, B. R. Inside Job: Methods for Delivering Proteins to the Interior of Mammalian Cells. *Cell Chem. Biol.* **2017**, *24* (8), 924−934.

(16) Cronican, J. J.; Beier, K. T.; Davis, T. N.; Tseng, J.-C.; Li, W.; Thompson, D. B.; Shih, A. F.; May, E. M.; Cepko, C. L.; Kung, A. L.; et al. A Class of Human Proteins that Deliver Functional Proteins into

Downloaded from pubs.acs.org/mpohbp/article-pdf/23/7/3722/6537496/acs.molpharmaceut.6c00191.pdf by WUHAN UNIV user on 20 September 2026

Mammalian Cells In Vitro and In Vivo. *Chem. Biol.* **2011**, *18* (7), 833−838.
(17) Hariton-Gazal, E.; Rosenbluh, J.; Graessmann, A.; Gilon, C.; Loyter, A. Direct translocation of histone molecules across cell membranes. *J. Cell Sci.* **2003**, *116* (22), 4577−4586.
(18) Rosenbluh, J.; Singh, S. K.; Gafni, Y.; Graessmann, A.; Loyter, A. Non-endocytic penetration of core histones into petunia protoplasts and cultured cells: a novel mechanism for the introduction of macromolecules into plant cells. *Biochim. Biophys. Acta Gen. Subj.* **2004**, *1664* (2), 230−240.
(19) Chan, A.; Tsourkas, A. Intracellular Protein Delivery: Approaches, Challenges, and Clinical Applications. *BME Front.* **2024**, *5*, 0035.
(20) Lawrence, M. S.; Phillips, K. J.; Liu, D. R. Supercharging Proteins Can Impart Unusual Resilience. *J. Am. Chem. Soc.* **2007**, *129* (33), 10110−10112.
(21) Cronican, J. J.; Thompson, D. B.; Beier, K. T.; McNaughton, B. R.; Cepko, C. L.; Liu, D. R. Potent Delivery of Functional Proteins into Mammalian Cells in Vitro and in Vivo Using a Supercharged Protein. *ACS Chem. Biol.* **2010**, *5* (8), 747−752.
(22) Cavazzini, D.; Spagnoli, G.; Mariz, F. C.; Reggiani, F.; Maggi, S.; Franceschi, V.; Donofrio, G.; Müller, M.; Bolchi, A.; Ottonello, S. Enhanced immunogenicity of a positively supercharged archaeon thioredoxin scaffold as a cell-penetrating antigen carrier for peptide vaccines. *Front. Immunol.* **2022**, *13*, 958123.
(23) Jacobs, M. I.; Bansal, P.; Shukla, D.; Schroeder, C. M. Understanding Supramolecular Assembly of Supercharged Proteins. *ACS Cent. Sci.* **2022**, *8* (9), 1350−1361.
(24) Bruce, V. J.; Lopez-Islas, M.; McNaughton, B. R. Resurfaced cell-penetrating nanobodies: A potentially general scaffold for intracellularly targeted protein discovery. *Protein Sci.* **2016**, *25* (6), 1129−1137.
(25) Der, B. S.; Kluwe, C.; Miklos, A. E.; Jacak, R.; Lyskov, S.; Gray, J. J.; Georgiou, G.; Ellington, A. D.; Kuhlman, B. Alternative computational protocols for supercharging protein surfaces for reversible unfolding and retention of stability. *PLoS One* **2013**, *8* (5), No. e64363.
(26) Yu, S.; Yang, H.; Li, T.; Pan, H.; Ren, S.; Luo, G.; Jiang, J.; Yu, L.; Chen, B.; Zhang, Y.; et al. Efficient intracellular delivery of proteins by a multifunctional chimaeric peptide in vitro and in vivo. *Nat. Commun.* **2021**, *12* (1), 5131.
(27) Arafiles, J. V. V.; Franke, J.; Franz, L.; Gómez-González, J.; Kemnitz-Hassanin, K.; Hackenberger, C. P. R. Cell-Surface-Retained Peptide Additives for the Cytosolic Delivery of Functional Proteins. *J. Am. Chem. Soc.* **2023**, *145* (45), 24535−24548.
(28) Wang, Q.; Yang, Y.; Liu, D.; Ji, Y.; Gao, X.; Yin, J.; Yao, W. Cytosolic Protein Delivery for Intracellular Antigen Targeting Using Supercharged Polypeptide Delivery Platform. *Nano Lett.* **2021**, *21* (14), 6022−6030.
(29) Yin, J.; Wang, Q.; Hou, S.; Bao, L.; Yao, W.; Gao, X. Potent Protein Delivery into Mammalian Cells via a Supercharged Polypeptide. *J. Am. Chem. Soc.* **2018**, *140* (49), 17234−17240.
(30) Ghosh, P. Boronic Acid-Linked Cell-Penetrating Peptide for Protein Delivery. *ACS Omega* **2024**, *9* (17), 19051−19056.
(31) Behzadipour, Y.; Hemmati, S. Covalent conjugation and non-covalent complexation strategies for intracellular delivery of proteins using cell-penetrating peptides. *Biomed. Pharmacother.* **2024**, *176*, 116910.
(32) Tai, W.; Zhao, P.; Gao, X. Cytosolic delivery of proteins by cholesterol tagging. *Sci. Adv.* **2020**, *6* (25), No. eabb0310.
(33) Georgiou, C. D.; Grintzalis, K.; Zervoudakis, G.; Papapostolou, I. Mechanism of Coomassie brilliant blue G-250 binding to proteins: a hydrophobic assay for nanogram quantities of proteins. *Anal. Bioanal. Chem.* **2008**, *391* (1), 391−403.
(34) Thompson, D. B.; Villaseñor, R.; Dorr, B. M.; Zerial, M.; Liu, D. R. Cellular Uptake Mechanisms and Endosomal Trafficking of Supercharged Proteins. *Chem. Biol.* **2012**, *19* (7), 831−843.
(35) Bragança, C. E.; Kraut, D. A. Mode of targeting to the proteasome determines GFP fate. *J. Biol. Chem.* **2020**, *295* (47), 15892−15901.
(36) Oviedo, M. J.; Quester, K.; Hirata, G. A.; Vazquez-Duhalt, R. Determination of conjugated protein on nanoparticles by an adaptation of the Coomassie blue dye method. *MethodsX* **2019**, *6*, 2134−2140.
(37) Le, Z.; Pan, Q.; He, Z.; Liu, H.; Shi, Y.; Liu, L.; Liu, Z.; Ping, Y.; Chen, Y. Direct Cytosolic Delivery of Proteins and CRISPR-Cas9 Genome Editing by Gemini Amphiphiles via Non-Endocytic Translocation Pathways. *ACS Cent. Sci.* **2023**, *9* (7), 1313−1326.
(38) Jeong, B. S.; Kim, H. C.; Sniezek, C. M.; Berger, S.; Kollman, J. M.; Baker, D.; Vaughan, J. C.; Gao, X. Intracellular delivery of proteins for live cell imaging. *J. Controlled Release* **2025**, *381*, 113651.
(39) Hall, M. P.; Unch, J.; Binkowski, B. F.; Valley, M. P.; Butler, B. L.; Wood, M. G.; Otto, P.; Zimmerman, K.; Vidugiris, G.; Machleidt, T.; et al. Engineered Luciferase Reporter from a Deep Sea Shrimp Utilizing a Novel Imidazopyrazinone Substrate. *ACS Chem. Biol.* **2012**, *7* (11), 1848−1857.
(40) England, C. G.; Ehlerding, E. B.; Cai, W. NanoLuc: A Small Luciferase Is Brightening Up the Field of Bioluminescence. *Bioconjugate Chem.* **2016**, *27* (5), 1175−1187.
(41) Liu, Y.; Ling, Y.; Tai, W. Mechanical Extrusion of the Plasma Membrane to Generate Ectosome-Mimetic Nanovesicles for Lung Targeting. *Mol. Pharmaceutics* **2025**, *22* (1), 304−315.
(42) Mao, Q.; Quan, Y.; Chen, S.; Tai, W. Design of bifunctional RNA-binding compounds that can modulate siRNA hydrophobicity for deep penetration and gene silencing in the retina. *Mol. Ther. Nucleic Acids* **2025**, *36* (4), 102751.
(43) Lazarenko, R. M.; DelBove, C. E.; Strothman, C. E.; Zhang, Q. Ammonium chloride alters neuronal excitability and synaptic vesicle release. *Sci. Rep.* **2017**, *7* (1), 5061.
(44) Bear, C. E.; Davison, J. S.; Shaffer, E. A. Intracellular pH influences the resting membrane potential of isolated rat hepatocytes. *BBA-Biomembranes* **1988**, *944* (2), 113−120.
(45) Fan, P.; Szerb, J. C. Effects of ammonium ions on synaptic transmission and on responses to quisqualate and N-methyl-D-aspartate in hippocampal CA1 pyramidal neurons in vitro. *Brain Res.* **1993**, *632*, 225−231.
(46) Cano-Ramirez, D. L.; Carmona-Salazar, L.; Morales-Cedillo, F.; Ramírez-Salcedo, J.; Cahoon, E. B.; Gavilanes-Ruíz, M. Plasma Membrane Fluidity: An Environment Thermal Detector in Plants. *Cells* **2021**, *10* (10), 2778.
(47) Ray, R.; Pal, S.; Das, S.; Jana, N. R. Direct Membrane Penetration and Cytosolic Delivery of Nanoparticles via Electrostatically Bound Amphiphiles. *ACS Appl. Mater. Interfaces* **2024**, *16* (13), 15819−15831.
(48) Allen, M. E.; Zhou, W.; Thangaraj, J.; Kyriakakis, P.; Wu, Y.; Huang, Z.; Ho, P.; Pan, Y.; Limsakul, P.; Xu, X.; et al. An AND-Gated Drug and Photoactivatable Cre-loxP System for Spatiotemporal Control in Cell-Based Therapeutics. *ACS Synth. Biol.* **2019**, *8* (10), 2359−2371.
(49) Matsuda, T.; Cepko, C. L. Controlled expression of transgenes introduced by in vivo electroporation. *Proc. Natl. Acad. Sci. U. S. A.* **2007**, *104* (3), 1027−1032.
(50) Harterink, M.; da Silva, M. E.; Will, L.; Turan, J.; Ibrahim, A.; Lang, A. E.; van Battum, E. Y.; Pasterkamp, R. J.; Kapitein, L. C.; Kudryashov, D.; et al. DeActs: genetically encoded tools for perturbing the actin cytoskeleton in single cells. *Nat. Methods* **2017**, *14* (5), 479−482.

Downloaded from pubs.acs.org/mpohbp/article-pdf/23/7/3722/6537496/acs.molpharmaceut.6c00191.pdf by WUHAN UNIV user on 20 September 2026

https://doi.org/10.1021/acs.molpharmaceut.6c00191
Mol. Pharmaceutics 2026, 23, 3722−3731